Provided for non-commercial research and education use.
Not for reproduction, distribution or commercial use.

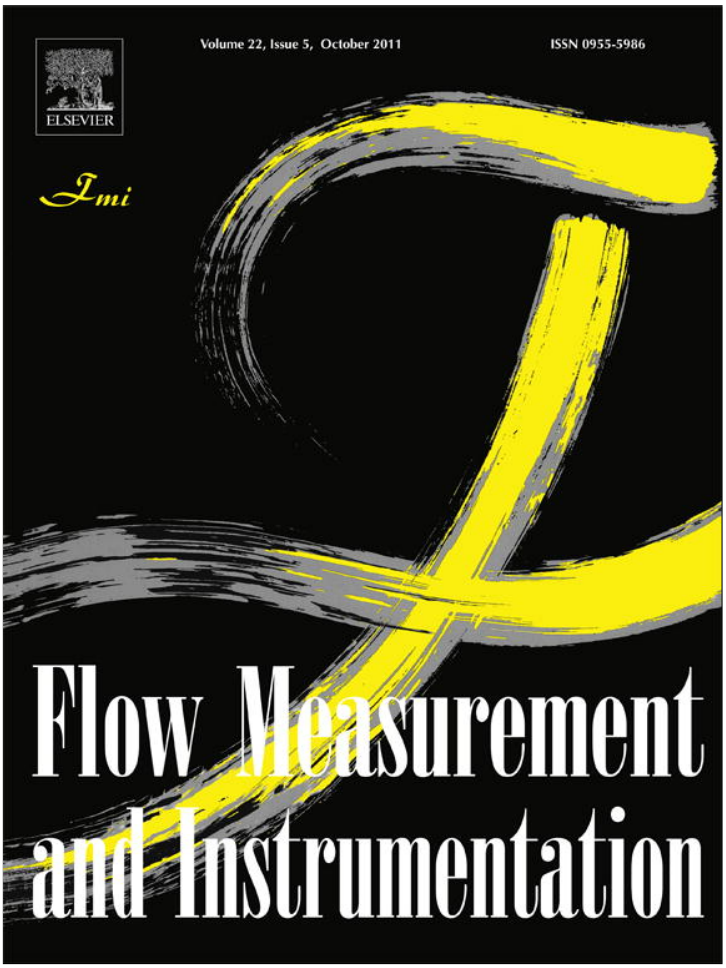

This article appeared in a journal published by Elsevier. The attached copy is furnished to the author for internal non-commercial research and education use, including for instruction at the authors institution and sharing with colleagues.

Other uses, including reproduction and distribution, or selling or licensing copies, or posting to personal, institutional or third party websites are prohibited.

In most cases authors are permitted to post their version of the article (e.g. in Word or Tex form) to their personal website or institutional repository. Authors requiring further information regarding Elsevier's archiving and manuscript policies are encouraged to visit:

http://www.elsevier.com/copyright

Author's personal copy

Flow Measurement and Instrumentation 22 (2011) 461–468

Contents lists available at SciVerse ScienceDirect

Flow Measurement and Instrumentation

journal homepage: www.elsevier.com/locate/flowmeasinst

Enhanced measurement capability of a digital particle holographic system for flow field measurements

Yan Yang [a], Boseon Kang [b,*]

[a] Key Laboratory of Automobile Parts and Test Techniques (Chongqing University of Technology), Ministry of Education, Chongqing, China
[b] Department of Mechanical Engineering, Chonnam National University, Gwangju, Republic of Korea

ARTICLE INFO

Article history:
Received 17 June 2010
Received in revised form
1 March 2011
Accepted 2 July 2011

Keywords:
Digital particle holography
Flow field
Correlation coefficient
Image binarization

ABSTRACT

To enhance the capability of digital particle holography as a tool for flow field measurements, several effective methods are developed. The correlation coefficient method was used to accurately locate the focal plane of particles and the optimal factors of this method were discussed. To remove noises and improve the quality of holograms and reconstructed images, the Wiener filter was adopted. The two-threshold and image segmentation methods were used to obtain high quality binary images from which we can get good results of particle extraction. Based on the above methods, an in-line digital particle holographic system was applied to channel flow field and the axial velocities of channel flow were measured. The feasibility of these methods is verified by quantitative measurement results which are in good agreement with the theoretical predictions.

© 2011 Elsevier Ltd. All rights reserved.

1. Introduction

Experimental investigation of flow fields is a key issue in fluid mechanics, but is limited by an inability to measure instantaneous three-dimensional (3D) flow field information. Laser Doppler Anemometry (LDA) can be used to measure the characteristics of a flow field, but it can only measure a point in the field [1]. Particle Image Velocimetry (PIV) and Particle Tracking Velocimetry (PTV) can detect particles in two-dimensional plane and overcome this problem [2]. Various extensions of 2D PIV such as Stereoscopic PIV [3] and Tomographic PIV [4] have been developed to measure 3D velocity vectors of flow fields. Especially, Tomographic PIV techniques using Multiplicative Algebraic Reconstruction Technique (MART) and Algebraic Reconstruction Techniques (ART) are good at implementation [5].

Holography is a method for recording and reconstructing the amplitude and phase of a wave [6]. Holography records the interference pattern between the object wave which is scattered by objects and the reference wave which directly arrives at the recording plane. A hologram is usually recorded on a flat surface, but contains information about the entire three-dimensional wave. This information is coded in the form of bright and dark micro-interferences, usually not visible to the human eye due to the high spatial frequencies. The object wave can be reconstructed by illuminating the hologram with the reference wave again. This reconstructed wave is indistinguishable from the original object wave. An observer sees a three-dimensional image that exhibits all the effects of perspective and depth of focus.

Since the 1960s, holography has been widely used to measure flow fields [7–11]. It can instantaneously capture the volumetric information of flow fields. Presently, digital holography, which rapidly replaced conventional holography, does not need a chemical process and has several benefits such as high efficiency, simplicity, and real time analysis. Therefore, digital holography has been widely used in the measurement of flow fields [12,13]. Due to the rapid development of charge coupled device (CCD) cameras and computer technologies, the quality of holograms has been improved and the computing speed of image reconstruction has been faster. Thus, digital particle holography has strong potential in measuring the features of flow fields.

In this study, a digital particle holographic system for flow field measurements is presented. To enhance the measurement capability of in-line digital particle holographic system for flow field, several effective methods, which are different from similar research [12–14], are developed. The correlation coefficient method is presented for focal plane determination of particles and the factors influencing this method are discussed. To remove noises and improve the quality of holograms and reconstructed images, the Wiener filter is introduced. The two-threshold and image segmentation methods are used in binary image transformation. The validation experiment for measurements of characteristics of laminar channel flow field is conducted. The basic shape of the flow velocity profiles are captured reasonably well and the errors between the experimental results and the theoretical predictions

* Corresponding author. Tel.: +82 62 5301683; fax: +82 62 5301689.
E-mail address: bskang@chonnam.ac.kr (B. Kang).

0955-5986/$ – see front matter © 2011 Elsevier Ltd. All rights reserved.
doi:10.1016/j.flowmeasinst.2011.07.001

Author's personal copy

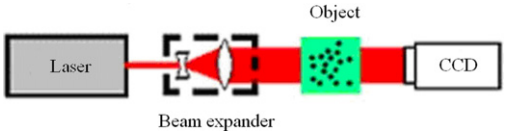

Fig. 1. Principle of in-line digital holography.

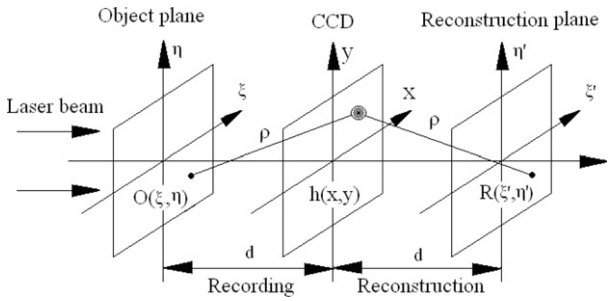

Fig. 2. The coordinate system.

can be acceptable. The experimental results showed that in-line digital particle holography can work well for measurements of flow fields based on proposed methods.

2. Theory and measuring principles

2.1. Theory of digital holography

Digital holography is classified as in-line or off-axis depending on the optical set-up. In-line digital holography is widely used because it has a simple optical configuration. The concept of in-line digital holography is shown in Fig. 1. Object beam and reference beam create an interference pattern on a CCD sensor, and this process can be described by the Fresnel–Kirchhoff integral [15]:

$$R(\xi',\eta') = \frac{\mathrm{i}}{\lambda}\int_{-\infty}^{\infty}\int_{-\infty}^{\infty} h(x,y)E_R(x,y)\frac{\exp\left(-\mathrm{i}\frac{2\pi}{\lambda}\rho\right)}{\rho}\mathrm{d}x\mathrm{d}y \qquad (1)$$

with

$$\rho = \sqrt{(\xi'-x)^2+(\eta'-y)^2+d^2} \qquad (2)$$

where $R(\xi',\eta')$, $h(x,y)$, $O(\xi,\eta)$, and $E_R(x,y)$ are functions of the reconstruction image, hologram, object, and reference, respectively. Here, d is the distance between two adjacent planes, λ is the wavelength, and ρ is the distance between two corresponding points in two adjacent planes. The coordinates appearing in Eqs. (1) and (2) are shown in Fig. 2. According to the object distance, holography is also classified as Fresnel (near field) or Fraunhofer (far field) holography. In this paper, Fresnel holography is investigated.

In optical holography, when the hologram is illuminated by a coherent wave known as the reconstruction wave which is the same as the reference beam, the reconstruction image will appear in the field of vision. In digital holography, the reconstruction process can be achieved by mathematical form and implemented in computer. The reconstruction image can be obtained by the Fresnel method or the convolution method [15]. In our previous analysis [16], the resolution of the reconstruction image by the convolution method was better than that by the Fresnel method. Therefore, the convolution method was used in this study.

2.2. Methods for enhanced measurement capability

2.2.1. Determination of focal plane

In digital particle holography, the x, y coordinates are easy to locate in high precision using common image processing method, regardless of the particles in focus or unfocused. The main problem is how to find the location of the best focal plane of particles along the optical axis, i.e. the z coordinate of particle. Various methods have been suggested to determine the focal plane. Lefebvre et al. [17] showed that the Maximum Modulus of Wavelet transform was reached at the best focal plane. Dubois et al. [18] introduced a method that uses the score of the integrated amplitude modulus. In our research group, Choo and Kang [19] proposed the correlation coefficient (CC) method to determine the focal plane of particles.

The correlation coefficient between reconstruction images measures the degree to which two reconstruction images are similar. The value of correlation coefficient approaches 0 if there is no similarity between reconstruction images and 1 if there is perfect similarity. The correlation coefficient is defined as

$$CC = \left[\frac{\sum_{m=1}^{M}\sum_{n=1}^{N}(F_{mn}-\bar{F})(G_{mn}-\bar{G})}{\sqrt{\left[\sum_{m=1}^{M}\sum_{n=1}^{N}(F_{mn}-\bar{F})^2\right]\left[\sum_{m=1}^{M}\sum_{n=1}^{N}(G_{mn}-\bar{G})^2\right]}}\right] \qquad (3)$$

where F and G are two images, m and n are the pixel indices, F_{mn} and G_{mn} are the gray levels of individual pixel of reconstruction images F and G, and $\bar{F}$ and $\bar{G}$ are the mean gray levels of F and G. Based on Eq. (3), the calculating program of the correlation coefficient values can be easily made by Matlab. In program, the image can be denoted by the matrix, so the value of F_{mn} and G_{mn}, F and G can be obtained easily after we import the image into program. Fig. 3 shows a schematic of how to determine the focal plane of particles by using correlation coefficients. A series of reconstruction images are reconstructed slice-by-slice with the reconstruction interval, Δz. The correlation coefficient at an arbitrary plane along the optical axis is evaluated by using two reconstruction images at the same distance as the half of correlation interval, $\Delta C_z/2$, from that plane.

The intensity distribution of reconstruction images along the z axis can be calculated based on the numerical simulation of particle holograms. After reconstructing many holograms with different particle sizes and object distances, the intensity distribution curves of reconstruction images were found to be the similar symmetrical shape, as shown in Fig. 4. Based on this kind of curves, the intensity of two symmetrical images at each side of the focal plane should be the same and the value of the correlation coefficient at the focal plane should be maximum. The focal plane (i.e. z coordinates of object) can be determined by choosing the peak point from the correlation coefficient curve.

For the optimal correlation interval, ΔC_z, the difference in the CC values at z_4 and z_7 positions in Fig. 3 should be big enough to easily obtain the peak. The difference in the CC values at z_4 and z_7 positions with the change of the correlation interval is shown in Fig. 5, which was obtained by the numerical simulation of holograms with a particle diameter, D_d, of 75 μm. At the correlation interval of 10 mm, the difference in the CC values at z_4 and z_7 positions is the biggest. The distribution of correlation coefficients with several correlation intervals is also shown in Fig. 6. At too large or too small correlation intervals, the focal plane cannot be determined accurately. Based on the above results, the optimal value of the correlation interval was chosen as $\Delta C_z = 10$ mm. At this interval, the curve looks more symmetrical, and the peak point

Author's personal copy

Table 1
Errors of focal plane determination by the CC method (Unit: μm).

Size, D_d (μm)	Object distance, d (mm)										
	150	160	170	180	200	210	220	230	240	300	400
16	10	0	0	0	0	0	0	0	0	−20	10
100	0	−10	0	0	0	−10	5	15	10	−20	30
300	0	0	0	0	0	0	0	−20	15	−30	30
500	−10	5	10	0	5	−10	10	20	20	−30	25

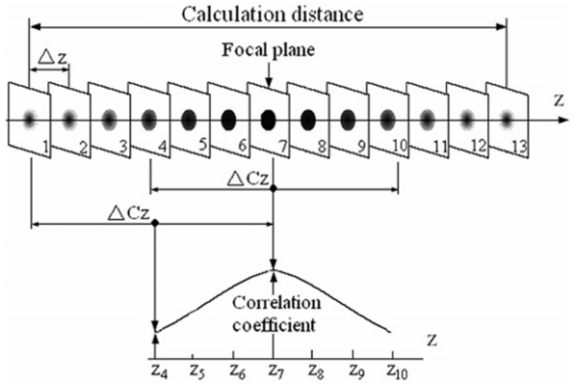

Fig. 3. Schematic diagram of correlation coefficient method.

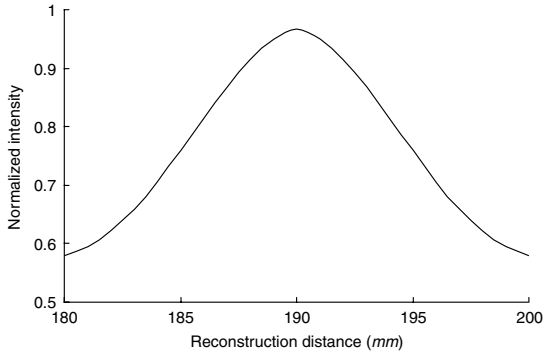

Fig. 4. Typical curve shape of intensity distribution of reconstruction images with particle size, $D_d = 300$ μm and object distance, $d = 190$ mm.

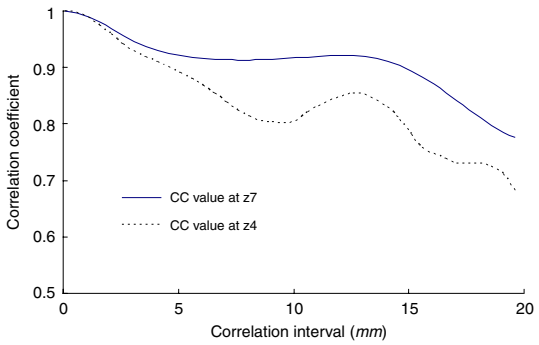

Fig. 5. Correlation coefficients by different correlation intervals (object distance, $d = 150$ mm).

considered as the focal point exactly agrees with the corresponding object distance.

After determination of the optimal correlation interval, the effects of the particle size, D_d, and the object distance, d, were investigated, as shown in Fig. 7. The smaller size particle gives better distinction than larger one in the correlation coefficient curve. The reason is that the depth of focus is proportional to the particle size so the change of small particle images is large around

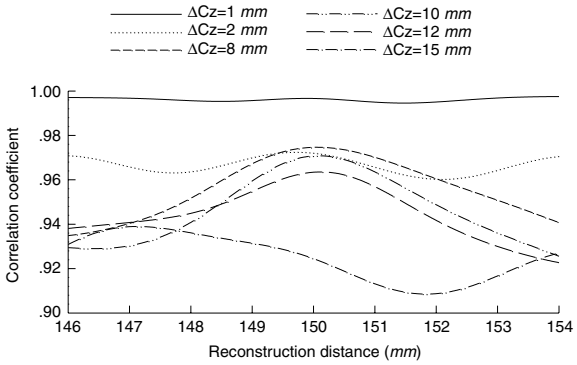

Fig. 6. Effect of correlation interval on correlation coefficient (object distance, $d = 150$ mm).

the focal plane. On the other hand, the images of large particles with large depth of focus do not change much within the given width around the focal plane. The errors at different particle sizes and object distances are shown in Table 1. The errors for the object distance between $d = 150$ and 220 mm are within acceptable range, but the errors for the objects located over $d = 220$ mm are large. Based on this result and the minimum object distance in Fresnel holography [15], the interval of the optimal object distance can be between $d = 150$ and 220 mm.

2.2.2. Noise removal

Actual digital holograms contain many inherent noises due to various optical conditions and dusts on components. Therefore, an image processing technique to eliminate these noises must be applied. To remove noises in holographic images, various filtering methods were examined including the inverse filter [20], the subtraction method [21], the Gaussian high-pass filter, and the spectral filter [22]. Among various filters considered, we adopted the self-adaptive Wiener filter [23] for pre-processing of digital holograms and post-processing of reconstruction images. The characteristics of the Wiener filter are shown in Fig. 8. The self-adaptive Wiener filter executes an optimal trade-off between inverse filtering and noise smoothing. It tailors itself to be the "best possible filter" for a given dataset by removing the additive noise and inverting the blurring simultaneously.

The in-line digital hologram of the dot array target was recorded to verify the feasibility of the Wiener filter in the CC method for focal plane determination. The dot array target and its hologram showing Regions of Interests (ROIs) of 81 dots are shown in Fig. 9. The application of the Wiener filter to an arbitrary dot is shown in Fig. 10. The Wiener filter works well to produce much better shape of the CC curve, from which the focal plane can be determined accurately.

2.2.3. Binarization of images

The reconstruction image of a hologram is the gray image, and it is difficult to extract the particles. Therefore, an image conversion process that converts gray images to binary images must be achieved. To obtain clear particle images, appropriate threshold values should be determined to transform gray images

Author's personal copy

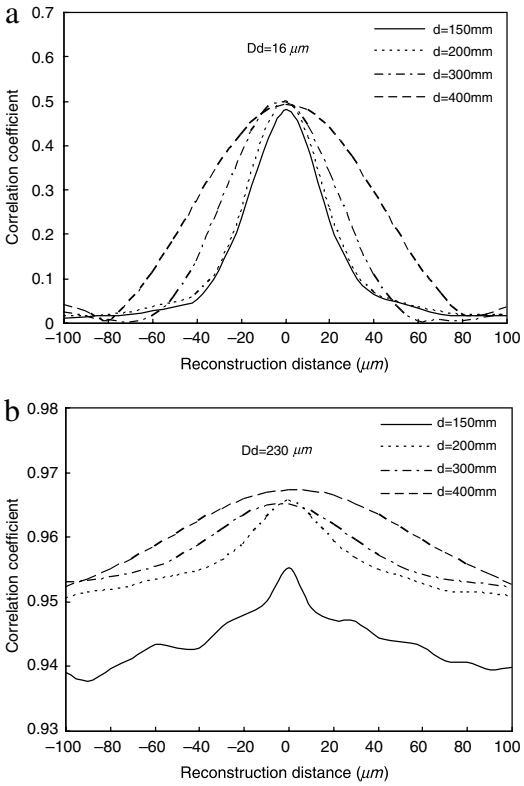

Fig. 7. Effect of particle size on correlation coefficient; (a) $D_d = 16\ \mu m$, (b) $D_d = 230\ \mu m$.

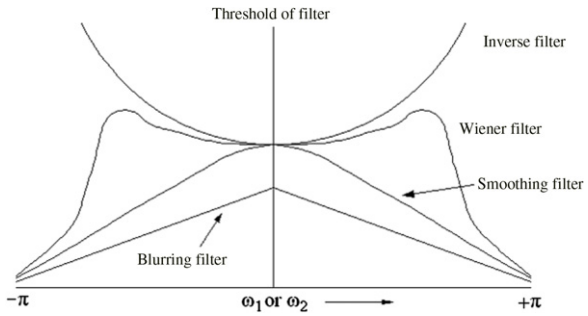

Fig. 8. Characteristics of self-adaptive Wiener filter.

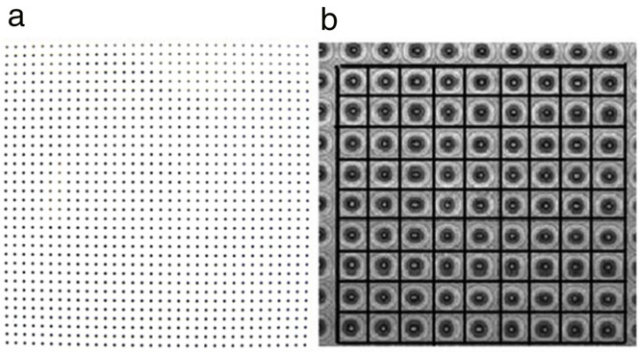

Fig. 9. Dot array target and its hologram: (a) Dot array target, (b) hologram of local target showing ROIs of 81 dots.

to binary images. In this study, the two-threshold method was applied to obtain the optimal threshold. The first threshold value,

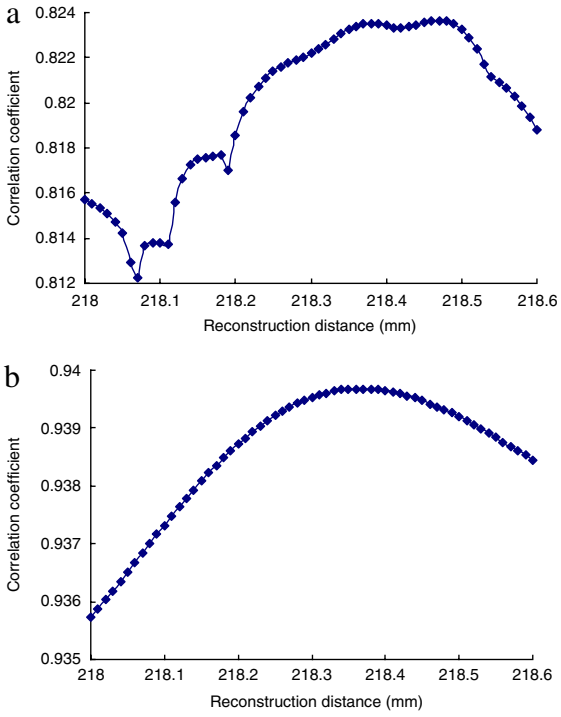

Fig. 10. Application of Wiener filter: (a) Without filtering, (b) with filtering.

I_{th1}, was obtained as follows:

$$I_{th1} = I_{1\min} + \bar{I}_1 \tag{4}$$

where $I_{1\min}$ and $\bar{I}_1$ are the minimum and average gray values of the reconstruction image, respectively. For the second threshold value, I_{th2}, the pixels whose gray values were under I_{th1} were selected first, comparing I_{th1} with the gray values of every pixel. The new minimum and average gray values of these pixels are $I_{2\min}$ and $\bar{I}_2$, respectively. The second threshold value is obtained as

$$I_{th2} = I_{2\min} + \bar{I}_2. \tag{5}$$

Using the second threshold value, we can transform gray images to binary images. In reconstruction images, the gray values of noises are usually higher than those of objects. The most of noises can be removed by using the two-threshold method instead of using single threshold value because the value of the latter is higher than that of the former which can efficiently match with objects. The procedure of the two-threshold method is shown in Fig. 11, which indicates its validity.

In our validation experiments, a reconstruction image of a calibration dot array target hologram was converted into the binary image using this method. The comparison results between the measured size and the actual size are shown in Fig. 12. The maximal and minimal errors of measured size with respect to the actual size were 7.3% and 0.2%, respectively, which proves the feasibility of the two-threshold method for image binarization.

Some useful information about particles can be lost if only one threshold is applied to the entire image because the intensity of the reconstruction image is not uniform. Thus, an image segmentation method was used in this study. The entire image was divided into several small regions that were converted to binary images using respective thresholds obtained by the two-threshold method. The comparison experiments clearly demonstrate that the image obtained by locally different thresholds was better than that by one threshold. The next problem is how to determine the optimal number of segmentations in one image. Comparison of results for different number of segmentations showed that the number

Author's personal copy

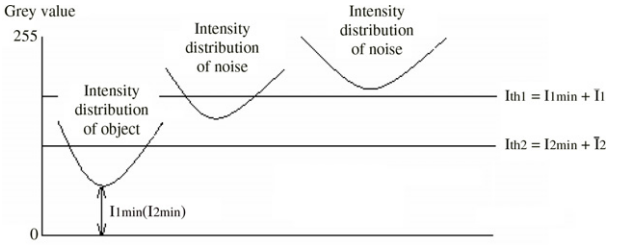

Fig. 11. Two-threshold method.

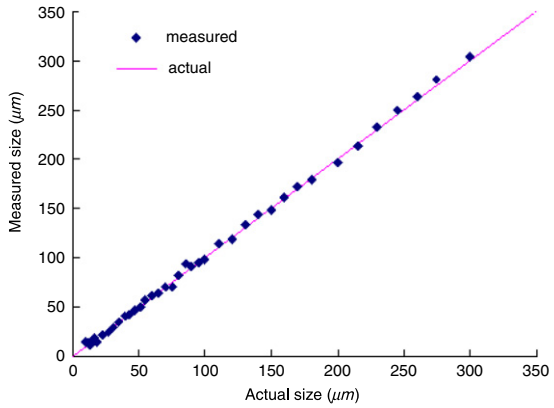

Fig. 12. Comparison of the measured size with the actual size.

is smaller and the quality of the conversion image is poorer. However, the increase of number of segmentations requires more calculation time. Considering all these factors, the optimum number of segmentations was chosen as 16. The comparison result by different number of segmentations is presented in Fig. 13.

3. Experiments

3.1. Object field and apparatus

Several enhanced features introduced in the previous section should be verified before application to complex three-dimensional flow field. For this purpose, the two-dimensional laminar channel flow was selected because it is easy and simple to conduct experiments and the measurement results can be easily compared with theoretical velocity profiles.

The velocity distribution of laminar channel flow in the fully developed region is well known and it can be approximated by Ebadian and Dong [24]:

$$\frac{U}{U_{\max}} = \left[1 - \left(\frac{y}{h/2}\right)^n\right]\left[1 - \left(\frac{z}{w/2}\right)^m\right] \tag{6}$$

where

$$\begin{aligned} m &= 1.7 + 0.5\alpha^{*-1.4} \\ n &= 2.0 \qquad\qquad\quad \text{for } \alpha^* \le 1/3 \\ n &= 2.0 + 0.3(\alpha^* - 1/3) \quad \text{for } \alpha^* \ge 1/3 \end{aligned} \tag{7}$$

and y and z are with respect to the center of the duct. $\alpha^* = h/w$ is the aspect ratio of the duct cross-section.

A digital particle hologram recording system for capturing flow field holograms was established as shown in Fig. 14. The laser through the beam expander extends to a plane beam that generates holograms on a CCD. After collecting the holograms from the CCD, the hologram image can be reconstructed, and information of flow field can be extracted. The specifications of the optical system components are as follows:

Laser: Nd-YAG laser (Quantel, wavelength 532 nm).
CCD camera: Megaplus II ES4020 (Kodak, pixel size 7.4 μm, pixel number 2048 × 2048, 15 fps).
Pulse generator: 555 (Berkeley, 4 channels, precision: 1 ns).
Translation system: M-531 (Physik Instrumente, precision: 33 nm).

3.2. Experimental procedure

A schematic diagram of the channel flow field measurement is shown in Fig. 15. To adequately validate feasibility of digital holography for measurement of flow field, the channel flow in two cross-section areas (15×15 and 20×20 mm^2) were investigated. The tracer particles are polymer particles about 50 μm in diameter. As shown in Fig. 15, water with tracer particles flowed in the x direction in the channel, which is made of plastic. The laser illuminated the channel in the $-z$ direction through the glass window, and then, holograms of tracer particles were captured.

Measurements were taken in the measuring section made from the glass window located downstream of a 0.8 m long settling length. Thus, fully developed flow can be assumed. To obtain enough particles for the analysis, six double exposure images (12 holograms) were continuously captured at the same flow rate conditions. The time interval between pulses was 0.1 s. The experimental conditions are shown in Table 2. The Reynolds number was based on the hydraulic diameter, $D_h = \frac{2hw}{(h+w)}$. Double exposure holograms of channel flow fields at different conditions were captured. All area of the 15×15 mm^2 cross-section in the x–y

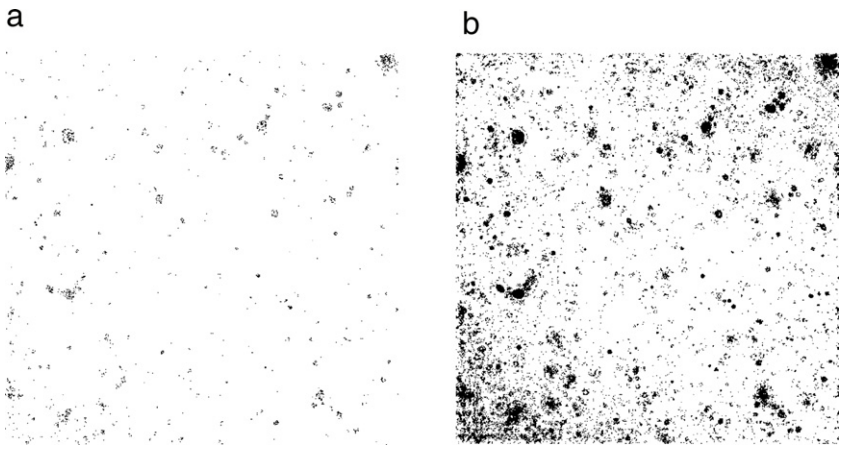

Fig. 13. Comparison of using different segmentations; (a) 1 segmentation, (b) 16 segmentations.

Author's personal copy

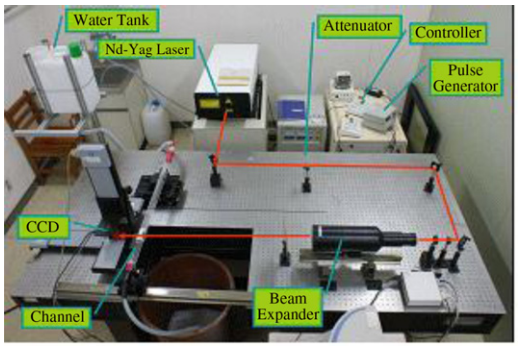

Fig. 14. Digital particle holographic system.

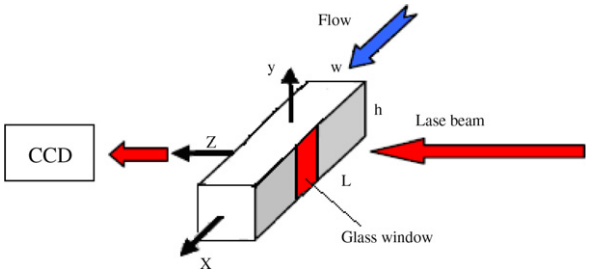

Fig. 15. Schematic diagram of channel flow field measurement.

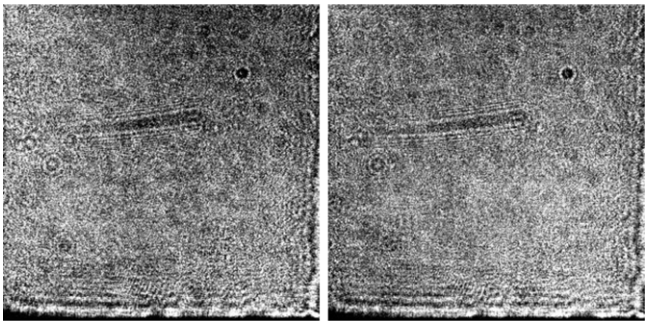

Fig. 16. Double exposure holograms of channel flow field.

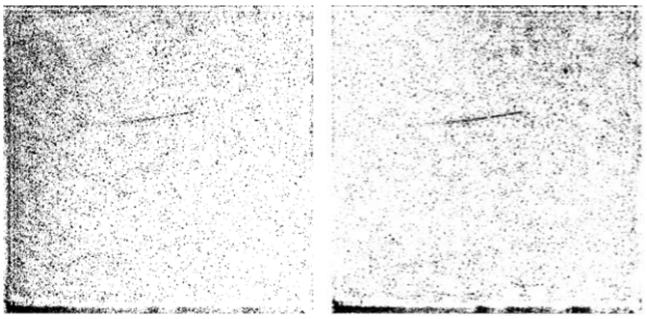

Fig. 17. Reconstruction images of Fig. 16.

plane was captured, but a part of the 20 × 20 mm^2 cross-section area was captured due to the limited CCD sensor size. Typical holograms and their reconstruction images are shown in Figs. 16 and 17, respectively.

3.3. Velocity extraction

To obtain the velocity distribution of the flow field, the measurement volume of the flow field is divided into i segments in x and y directions, respectively, as shown in Fig. 18. The number

Table 2
Experimental conditions.

Area (mm^2)	Re	V_{ave} (mm/s)
15 × 15	111	7.4
	377	25.2
	622	41.4
20 × 20	83	4.2
	282	14.2
	467	23.3

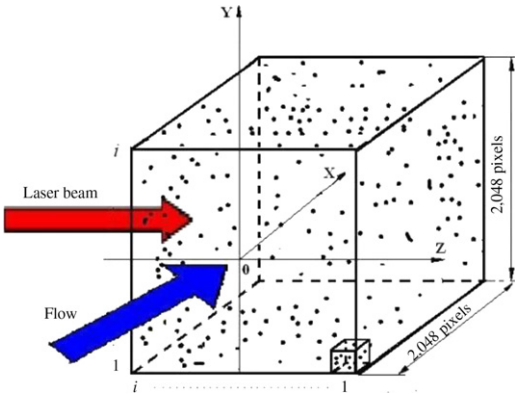

Fig. 18. Measurement volume and small cube of flow field.

of segments is 14 and 19 for 15 × 15 and 20 × 20 mm^2 cross-section areas, respectively. Then, many cuboids are obtained. By using the cross-correlation method and analyzing the particles in corresponding cuboids in double exposure holograms, the mean velocity of particles in each cuboid is obtained. Combining all cuboids, the velocity distribution of the flow field is obtained. The details of the hologram image processing procedure are as follows:

(1) The measurement volume of the flow field is divided into many small cuboids.
(2) A Wiener filter is used to eliminate noises in the holograms.
(3) After determination of the focal plane using the CC method, the 3D coordinates of all particles in hologram are extracted. The distribution of particles in each cube is obtained by selecting all particles located in each cube. A reconstruction image with the distance from CCD to the center plane of the cube is reconstructed. And then, binary images are obtained by appropriate threshold and image segmentation methods. Even though some particle images are defocused at the reconstruction plane, they also can be included in the image and used to calculate the axial velocity because all of them are in one small cube and they can present the velocity of this cube.
(4) After obtaining two binary images of each cuboid pair in double exposure images, the conventional cross-correlation method in PIV is performed. The size and the orientation of the interrogation windows are determined according to the particle size, cuboid size, and flow direction. In this study, the window size was 64 × 64 pixels. By calculating the cross-correlation of binary particle images in two cuboids, the velocity vector in this cuboid is obtained. Then, the mean velocity in the axial direction of this cuboid is obtained.
(5) Repeat the procedure of step (4) until the mean axial velocities of every cuboid are obtained and the axial velocity profiles are achieved.

4. Results and discussion

After analyzing the double exposure holograms of channel flow field for different Reynolds numbers, the axial velocity profiles for

Author's personal copy

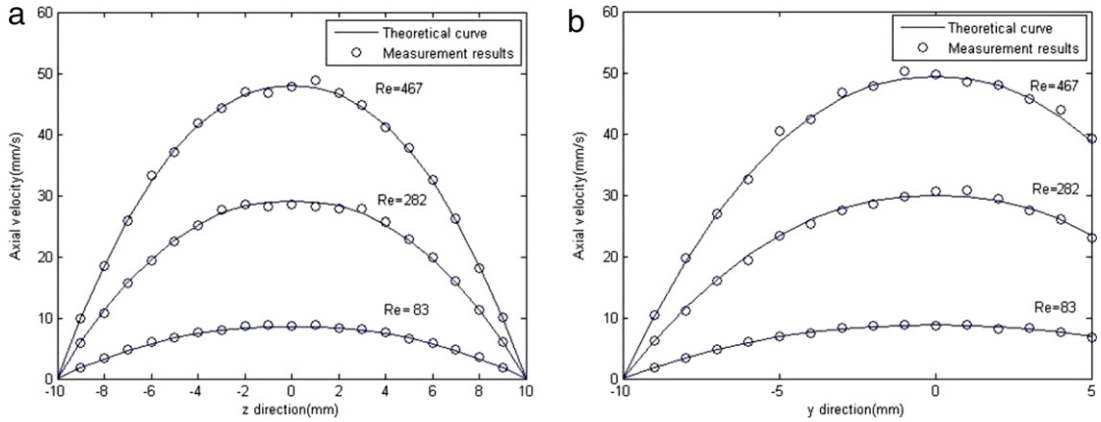

Fig. 19. Axial velocity profiles in the middle of channel for channel size 20 × 20 mm^2; (a) x–z (horizontal) plan, (b) x–y (vertical) plane.

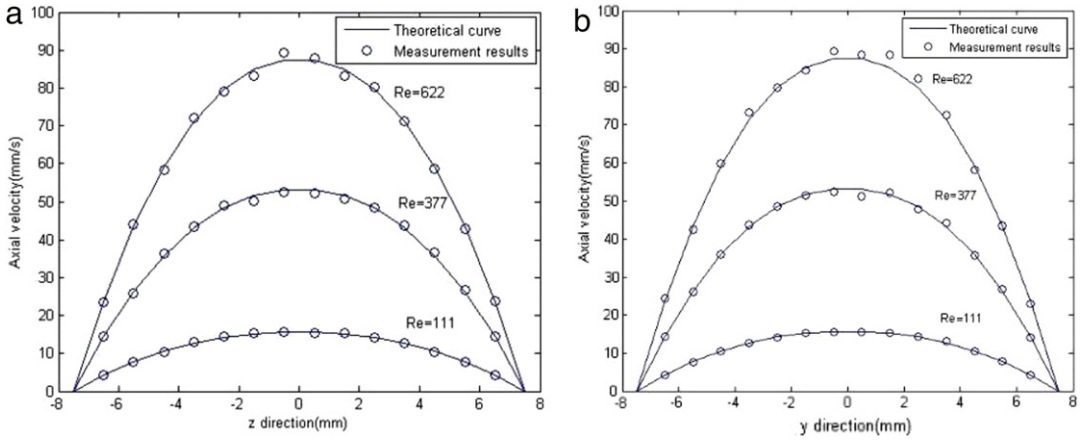

Fig. 20. Axial velocity profiles in the middle of channel for channel size 15 × 15 mm^2; (a) x–z (horizontal) plan, (b) x–y (vertical) plane.

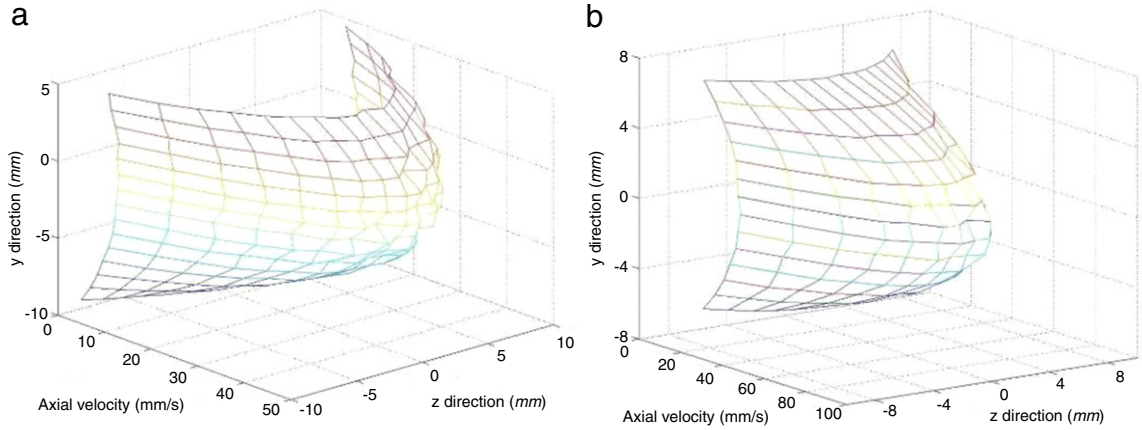

Fig. 21. 3D flow velocity profiles; (a) channel area 20 × 20 mm^2, Re = 467; (b) channel area 15 × 15 mm^2, Re = 622.

different channel sizes are shown in Figs. 19 and 20. The typical 3D flow velocity profiles are shown in Fig. 21. All velocity profiles are in good agreement with the theoretical predictions.

Although the basic shape of the profile was captured reasonably well, Figs. 17 and 18 reveal some imperfections in the experimental profile. There are some deviations between the experimental and the theoretical profiles at the center region of the profile. The surface at the center region is not smooth, which was caused by the cross-correlation method. In addition, the degree of precision of the focal plane determination is also a part of these imperfections.

The magnitude of errors for every case is shown in Table 3. The error is defined as the difference between the theoretical values and the measured values. The maximum errors, the mean value of all errors, and the mean error with respect to the average velocity of each case are shown in the table. The relationship between the Reynolds number and the measurement error is shown in Fig. 22. In Fig. 20 and Table 3, we can note that the absolute errors are directly proportional to the Reynolds number in the same channel. As the velocity increases, the errors of particle position and pairing increase. Nevertheless, the relative mean errors with respect to

Author's personal copy

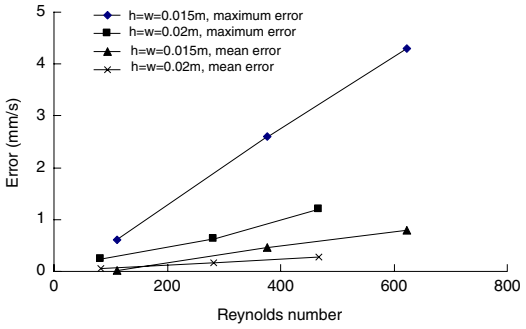

Fig. 22. Measurement errors.

Table 3
Errors in velocity measurements (Unit: mm/s).

Area (mm^2)	Re	Max. error	Mean error	Mean error/V_{ave} × 100 (%)
	111	0.6	0.01	0.14
15 × 15	377	2.6	0.46	1.83
	622	4.3	0.79	1.91
	83	0.2	0.05	1.19
20 × 20	282	0.6	0.17	1.20
	467	1.2	0.28	1.20

the average velocity are within a maximum of 2%, which can be acceptable. These results suggest that the proposed features of the digital particle holographic system work well. Application of the developed system to more complex 3D flow field remains as a future work.

5. Conclusions

Digital in-line particle holography is a tool well adapted to measure the characteristics of flow fields. In this study, some effective methods to enhance the measurement capability of digital particle holography for flow field are developed. The correlation coefficient method was introduced to determine the focal plane of particles in high precision and the optimal values of parameters, i.e., the particle size, the object distance, and the correlation interval, were discussed. The error of focal plane determination increased with the particle size. The optimal object distance was from 150 to 220 mm and the optimal correlation interval was 10 mm. For noise removal in digital particle holography, the Wiener filter was applied to the hologram and the reconstruction image. Experimental results proved that this filter can efficiently remove noise and increase the precision of focal plane location by the correlation coefficient method. For post-processing of reconstruction images, the two-threshold method and the image segmentation technique were presented and used effectively in binary image transformation. Most of noises can be removed well by using the two-threshold method instead of single threshold value. The number of segmentations is directly proportional to the quality of the conversion image. Considering the calculation time and the quality of binary image, the optimum number of segmentations was chosen as 16.

Based on these methods with optimal parameters, the double exposure holograms of channel flow field in different cases were captured by the in-line digital particle holographic system and the holograms were effectively processed. All experimental results are good agreement with the theoretical profiles. The errors are directly proportional to the flow velocity and the Reynolds number, but the value of them can be acceptable. The results show digital particle holography can be regarded as a satisfied tool for flow field measurements by using these methods proposed in this study.

Acknowledgments

This work was supported by the Korea Research Foundation Grant funded by the Korean Government (KRF-2008-313-D00137), by the Natural Science Foundation Project of CQ CSTS (2010BB2087), by the Natural Science Foundation Project of CQEC (KJ110822), and by the Priming Scientific Research Foundation of CQUT(2009zd29).

References

[1] Durst F, Melling A, Whitelaw JH. Principles and practices of laser-doppler anemometry. London: Academic Press; 1981. p. 86–104.
[2] Stitou A, Riethmuller ML. Extension of PIV to super resolution using PTV. Meas Sci Technol 2001;12:1398–403.
[3] Fei R, Merzkirch W. Investigations of the measurement accuracy of stereo particle image velocimetry. Exp Fluids 2004;37:559–65.
[4] Kim MK. Tomographic three-dimensional imaging of a biological specimen using wavelength-scanning digital interference holography. Opt Exp 2000;7:305–10.
[5] Elsinga GE, Scarano F, Wieneke B, van Oudheusden BW. Tomographic particle image velocimetry. Exp Fluids 2006;41:933–47.
[6] Gabor D. A new microscopic principle. Nature 1948;161:777–8.
[7] Pan G, Meng H. Digital in-line holographic PIV for 3D particulate flow diagnostics. In: Proceeding of 4th international symposium on PIV 2001; PIV'01 Paper 1008. p. 1-5.
[8] Scherer JO, Bernal LP. In-line holographic particle image velocimetry for turbulent flows. Appl Opt 1997;36:9309–18.
[9] Meng H, Hussain F. In-line recording and off-axis viewing technique for holographic particle velocimetry. Appl Opt 1995;34:1827–40.
[10] Thompson BJ. Diffraction by opaque and transparent particles. J SPIE 1963;2:43–6.
[11] Trolinger JD, Beltz RA, Farmer WM. Holographic techniques for the study of dynamic particle fields. Appl Opt 1969;8:957–61.
[12] Pan G, Meng H. Digital in-line holographic PIV for 3D particulate flow diagnostics. In: 4th international symposium on particle image velocimetry. 2001.
[13] Malek M, Allano D, Coëtmellec D, Lebrun D. Digital in-line holography: influence of the shadow density on particle field extraction. Opt Exp 2004;12:2270–9.
[14] Soria J, Atkinson C. Towards 3C-3D digital holographic fluid velocity vector field measurement – tomographic digital holographic PIV (Tomo-HPIV). Meas Sci Technol 2008;19: 074002.1–12.
[15] Schnars U, Jueptner W. Digital holography. Berlin: Springer; 2005. p. 41–53.
[16] Yang Y, Kang BS. Application of digital holography to sprays. Proc Asia Display 2007;2050–4.
[17] Lefebvre CB, Coëtmellec S, Lebrun D, COzku L. Application of wavelet transform to hologram analysis: three-dimensional location of particles. Opt Laser Eng 2000;33:409–21.
[18] Dubois F, Schockaerts C, Callen N, Yourassowsky C. Focus plane detection criteria in digital holography microscopy by amplitude analysis. Opt Exp 2006;14:5895–980.
[19] Choo YJ, Kang BS. The characteristics of the particle position along an optical axis in particle holography. Meas Sci Technol 2006;17:761–70.
[20] Denis L, Fourner T, Ducottet C. Twin-image noise reduction by phase retrieval in in-line digital holography. Proc SPIE 2005;5914:148–61.
[21] Salah N, Godard G, Lebrun D, Paranthoën P, Allano D, Coëtmelle S. Application of multiple exposure digital in-line holography to particle tracking in a Bénard–von Kármán vortex flow. Meas Sci Technol 2008;19: 07401.1–9.
[22] Kim S, Lee SJ. Effect of particle concentration on digital holographic PTV measurement. J Korea Soc Mech Eng B 2006;30:929–34.
[23] Jain AK. Fundamentals of digital image processing. USA: Prentice-Hall; 1989. p. 276–306.
[24] Ebadian MA, Dong ZF. Handbook of heat transfer. USA: McGraw Hill; 1989. p. 100–31.